JOURNAL OF GEOPHYSICAL RESEARCH, VOL. 114, A00C22, doi:10.1029/2009JA014114, 2009

Substorm current wedge driven by plasma flow vortices: THEMIS observations

A. Keiling,[1] V. Angelopoulos,[2] A. Runov,[2] J. Weygand,[2] S. V. Apatenkov,[3] S. Mende,[1] J. McFadden,[1] D. Larson,[1] O. Amm,[4] K.-H. Glassmeier,[5] and H. U. Auster[5]

Received 29 January 2009; accepted 23 February 2009; published 27 May 2009.

[1] A multipoint analysis of conjugate magnetospheric and ionospheric flow vortices during the formation of the substorm current wedge (SCW) on 19 February 2008 is presented. During the substorm, four Time History of Events and Macroscale Interactions during Substorms (THEMIS) spacecraft were located close to the neutral sheet in the premidnight region between 9 and 12 R_E geocentric distance, of which three closely ($\sim$1–2 R_E) clustered at $\sim$23 MLT and one was farther west at $\sim$21 MLT. The closely clustered spacecraft were engulfed by a counterclockwise plasma flow vortex, while the single spacecraft recorded a clockwise plasma flow vortex. Simultaneously, a pair of conjugate flow vortices with clockwise and counterclockwise rotation appeared in the ionosphere, as inferred from equivalent ionospheric currents. The counterclockwise space vortex, which corresponded to a downward field-aligned current, was at least 1–2 R_E in diameter and had rotational flow speeds of up to 900 km/s. Current density estimates associated with the formation of the space vortex in the first 30 s yielded 2.8 nA/m^2 (14 μA/m^2 mapped to the ionosphere), or a total current of 1.1 $\times$ 10^5 A. Model calculations based on midlatitude ground magnetometer data show a gradual increase of the field-aligned current, with 1–2 $\times$ 10^5 A within the first minute and a peak value of 7 $\times$ 10^5 A after 10 min, associated with the SCW, and a matching meridian of the downward current of the SCW and the downward current (counterclockwise) space vortex. The combined ground and space observations, together with the model results, present a scenario in which the space vortices generated the field-aligned current of the SCW at the beginning of the substorm expansion phase and coupled to the ionosphere, causing the ionospheric vortices.

Citation: Keiling, A., et al. (2009), Substorm current wedge driven by plasma flow vortices: THEMIS observations, *J. Geophys. Res.*, *114*, A00C22, doi:10.1029/2009JA014114.

1. Introduction

[2] The substorm current wedge (SCW) is a current system that forms during substorms [e.g., *McPherron*, 1979], and electrically couples the near-Earth plasma sheet with the ionosphere via (at least) one pair of downward and upward field-aligned currents (FACs). These FACs cause a multitude of phenomena during the course of a substorm, one of which is the substorm-related aurora. An understanding of the formation of this current system is of key importance for an understanding of the substorm phenomenon as a whole. Two sources for the SCW have been suggested, namely the inertial current and the pressure gradient current, both of which are perpendicular currents and are believed to be diverted to form the field-aligned portion of the SCW:

$$\mathbf{j}_\perp = \frac{\mathbf{B}}{B^2} \times \rho \frac{d\mathbf{u}}{dt} + \frac{\mathbf{B}}{B^2} \times \nabla P \tag{1}$$

The inertial current, first term on the right-hand side, is considered to be more relevant for the generation of FAC during the initial dynamic phase of substorms [*Haerendel*, 1992; *Shiokawa et al.*, 1997]. Equation (1) does not show, however, how the perpendicular current is diverted into the field-aligned direction, and how much of it is diverted. Alternatively, starting from equation (1) and using $\nabla_\parallel \bullet \mathbf{J}_\parallel = -\nabla_\perp \bullet \mathbf{J}_\perp$, a direct expression for the FAC due to the change of vorticity and the magnetic field can be derived [*Hasegawa and Sato*, 1979]:

$$j_\parallel = B_i \int_{eq}^{ion} \frac{\rho}{B} \frac{d}{dt} \left(\frac{\Omega}{B} \right) dl_\parallel, \tag{2}$$

where Ω is the vorticity, B is the magnetic field (subscript "i" refers to the ionosphere), ρ is the mass density, and the

[1]Space Sciences Laboratory, University of California, Berkeley, California, USA.
[2]IGPP, University of California, Los Angeles, California, USA.
[3]Institute of Physics, St. Petersburg State University, St. Petersburg, Russia.
[4]Finnish Meteorological Institute, Helsinki, Finland.
[5]IGEP, Technical University of Braunschweig, Braunschweig, Germany.

0148-0227/09/2009JA014114$09.00

integration is along the magnetic field line from the equator to the ionosphere to obtain the current density at the top of the ionosphere. The derivation yields additional terms, which can contribute to the FAC, one of which is

$$j_{\parallel} = B_i \int_{eq}^{ion} \frac{2}{B^2} \mathbf{j}_{\perp} \cdot \nabla B \, dl_{\parallel} \tag{3}$$

and accounts for the spatial variation of the magnetic field in the direction of the perpendicular current. Whereas *Hasegawa and Sato* [1979] argued that (2) is the dominant cause of the FAC during the dynamic phase of substorms, *Lui* [1996] argued for (3). We note that (2) can be derived from the inertial current term in equation (1) alone, whereas (3) requires both terms in equation (1). The focus in this report is the FAC generation due to flow vorticity. Several substorm scenarios, such as plasma flow breaking/diversion and magnetic pileup [e.g., *Shiokawa et al.*, 1997; *Birn et al.*, 1999], cross-field current instability [e.g., *Lui et al.*, 1991; *Lui*, 1996], and ballooning instabilities of various types [e.g., *Voronkov et al.*, 1997; *Bhattacharjee et al.*, 1998], allow for the formation of flow vorticity and associated FAC generation (among other FAC generation mechanisms). The significance of the vortex mechanism operating in the magnetotail has also been suggested from MHD simulations [*Birn and Hesse*, 1996; *Ashour-Abdalla et al.*, 2002].

[3] Vortical plasma flows also exist in the ionosphere [e.g., *Kosch et al.*, 1998], and it is thought that they are created by plasma flow vortices in space [e.g., *Borovsky and Bonnell*, 2001]. Thus the ionospheric flow vortex forms an image of activity in the magnetosphere [*Akasofu*, 1976], and one attempts to infer properties of the magnetospheric flow vortex from ground data. Direct observational evidence for this connection, however, does not exist, partly due to the difficulty of finding conjunctions and, if one is found, it is questionable as to how accurate the estimate for the conjunction is. Furthermore, single-spacecraft measurements of possible vortical structures in space must be considered ambiguous because of the multitude of activities occurring during substorms. In steady state, vorticity is conserved along field lines, in which case one might infer much about the magnetospheric vortex from ionospheric vortex observations [e.g., *Pudovkin et al.*, 1997]. On scales of the Alfvén transit times (~1 min), dynamic changes need to be considered [e.g., *Pudovkin et al.*, 1997]. Thus vortices related to substorms, which have time scales of minutes, clearly require a dynamical approach. Ultimately, conjugate multipoint observations of the magnetospheric source region and the ionosphere need to be provided to determine the coupling properties in comparison with simulation models and theory.

[4] Vortex structures are also identified in equivalent ionospheric currents (EICs) [e.g., *Untiedt et al.*, 1978; *Küppers et al.*, 1979], which can in turn be interpreted as ionospheric plasma flow vortices. Under the assumption of uniform ionospheric conductance, the EICs equal the Hall currents which flow in the $-(\mathbf{E} \times \mathbf{B})$ direction. Hence, the opposite of the EIC direction yields an estimate of the convectional flow direction. Both clockwise and counterclockwise rotations of EIC vortices when viewed along the magnetic field direction exist and are associated with downward and upward field-aligned currents (FACs), respectively [*Untiedt et al.*, 1978; *Opgenoorth et al.*, 1980]. EIC vortices have been reported during both substorm expansion and growth phase [e.g., *Steen and Collis*, 1988; *Lyatsky et al.*, 2001; *Weygand et al.*, 2008], and during the sudden brightening of an auroral arc [*Kosch et al.*, 1998]. Evidence suggests that some EIC vortices are collocated with the substorm surge [*Lyatsky et al.*, 2001].

[5] In this report, we present a multisatellite, observation-based comparison of conjugate magnetospheric and ionospheric vortices (via EICs), and we demonstrate that the ionospheric vortices were driven by the space vortices. Moreover, evidence is given that the space vortices contributed to the field-aligned current of the SCW by applying equation (2) and by comparison with model results of a reconstructed SCW. Properties of one space vortex are described using multipoint measurement from the Time History of Events and Macroscale Interactions during Substorms (THEMIS) spacecraft [*Angelopoulos*, 2008; *Sibeck and Angelopoulos*, 2008; *Bester et al.*, 2008; *Auster et al.*, 2008; *McFadden et al.*, 2008; D. Larson et al., Solid state telescope for THEMIS, manuscript in preparation, 2009). Optical data of the aurora and ground magnetometer data were obtained from THEMIS's ground-based observatories [*Mende et al.*, 2008; *Russell et al.*, 2008].

2. Event: 19 February 2008

2.1. Ground-Based Observations

[6] On 19 February 2008, an isolated substorm occurred with onset at approximately 0525 UT, as evidenced in the *H* component of ground magnetometer data (Figure 1). A negative *H* bay was first recorded at Fort Smith (FSMI) and then expanded westward and eastward with the most intense deflection (~500 nT) near Gillam (GILL) and Rankin Inlet (RANK). The locations of the ground stations are shown in Figure 2. The auroral onset and expansion are seen in the selected sequence of all-sky images (ASI) (Figure 2; note that the bright spot in each ASI image is the Moon). The expansion was poleward, westward, and strongly eastward with an estimated (from ASI images) speed of the brightening region of 9 km/s. At 0525:41 UT, a very prominent auroral spiral had formed while curling up counterclockwise. The red dots in Figure 2 (top left) mark the proximate locations of the THEMIS spacecraft footprints using the T96 magnetospheric model [*Tsyganenko*, 1995]. Thus, the onset location was between TH-C and the group of three spacecraft (TH-A, D, and E). The corresponding space signatures are shown in section 2.2.

[7] Figure 3 shows equivalent ionospheric currents (EICs) derived from a matrix inversion technique that uses the measured ground magnetic disturbance of the THEMIS ground magnetometer array. This technique is described by *Amm* [1997] and *Amm and Viljanen* [1999]. The vectors indicate the current direction and intensity (scale is shown in the bottom right corner of each plot and varies among plots). Before 0525 UT, the EICs were relatively weak except of a stronger eastward electrojet. From 0525 UT to 0530 UT, the westward (substorm) EIC electrojet formed and intensified. Simultaneously, two EIC vortices with opposite rotational sense and approximate size of 600–800 km formed. Clockwise and counterclockwise rotations

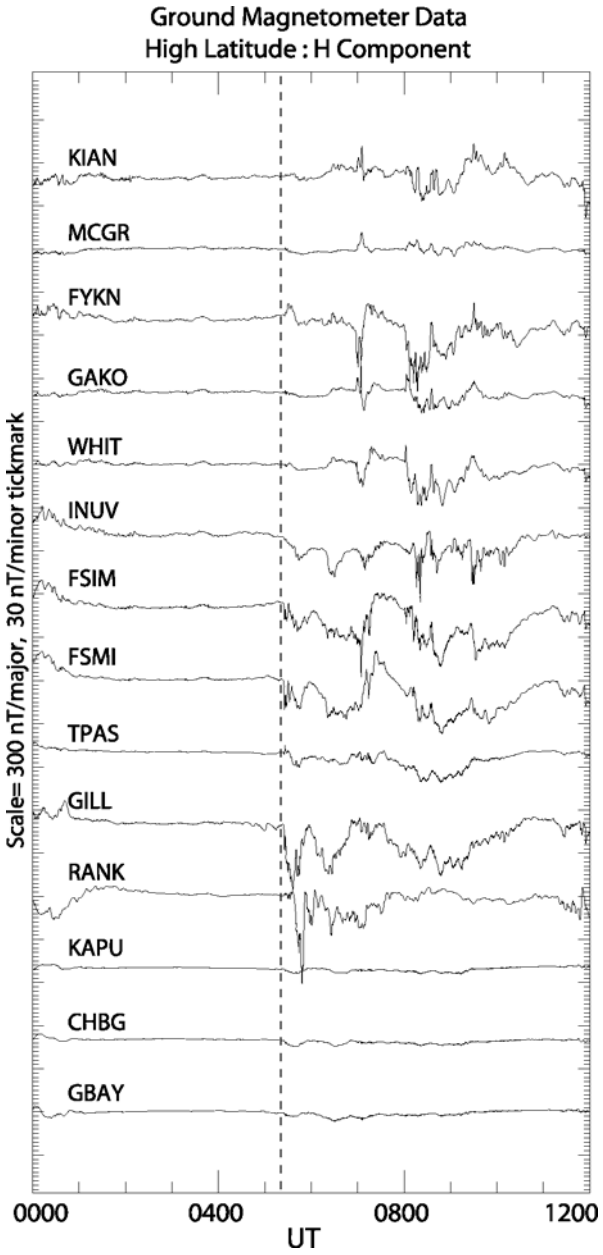

Figure 1. Ground magnetometer data (*H* component) on 19 February 2008. The dashed line marks the substorm onset.

correspond to downward and upward FAC, respectively. The yellow and red circles approximately mark the center of each vortex, which is not necessarily the center of the associated FAC, depending on the detailed distribution of the ionospheric conductance [e.g., *Kosch et al.*, 2000]. The upward current vortex was connected at its poleward rim to the onset region of the brightening aurora. Immediately after the auroral onset, both the auroral brightening region and the upward current vortex moved eastward (note the changing location of the yellow circle). The downward current vortex remained approximately at the same location until 0530 UT. It is also noted that the intense auroral spiral mentioned earlier formed between both EIC vortices, a region of intense currents and flows, approximately at the time when they reached their closest separation.

[8] The reconstructed SCW using THEMIS and INTERMAGNET ground magnetometer data is shown in Figure 4. The longitudinal locations of upward and downward FACs, as well as their magnitude as a function of time were modeled to fit the midlatitude magnetic field variations [*Horning et al.*, 1974; *Sergeev et al.*, 1996]. The current wedge started to develop at approximately 0525 UT with the upward and downward currents located at ~20.5 MLT and ~23 MLT, respectively. The meridian of the downward current coincided with those of the footprints of TH-A, D and E (labels a, d, and e) and the clockwise EIC vortex (downward current). The current magnitude gradually increased and reached its peak value $\sim 7 \times 10^5$ A at 0535 UT. The current longitudes fluctuated within 0.5 h MLT around their initial locations until ~0545 UT.

2.2. Space Observations

[9] At the time of auroral onset, the five THEMIS spacecraft were located in the nightside magnetosphere (Figure 5). TH-C was at ~21 MLT and ~11 R_E radial distance. TH-A, D, and E were closely clustered around 23 MLT and 9.5 to 12 R_E with separations in the X-Y (GSM) plane of ~1–2 R_E while their Z (GSM) separation was <0.2 R_E. Here we do not consider TH-B because it was located too far to the east for the purpose of this study. The four spacecraft were inside the plasma sheet and close to the neutral sheet. Plasma flow data and magnetic field data (Figure 5) show that in space, a disturbance was first observed at TH-C and then at TH-D, E, and A. All the spacecraft recorded dipolarizations (see B_z components). While TH-C, D, and E recorded strong plasma flow in the positive X direction (GSM), TH-A recorded strong flow in the negative X direction. The flows of the clustered spacecraft (TH-A, D, and E) show characteristics of a counterclockwise vortex, when viewed along the magnetic field direction, which is demonstrated below. This space vortex temporally and spatially coincided with the EIC vortex associated with the downward current (compare section 2.1). TH-C also recorded the signature of a passing vortex of opposite sense, as shown below.

[10] Figure 6 shows the temporal variations of the plasma flows in the X-Y plane (GSM). To the right, the flow vectors for four THEMIS spacecraft are plotted versus time. Numbered dashed lines mark the times for which the flow vectors are placed at the spacecraft locations in the X-Y (GSM) plane to the left in Figure 6. The flow vectors at TH-A, D, and E initially indicate steady azimuthal westward flow (#1, #2, and earlier times), whereas at TH-C the flow direction is variable. At #3, the flow at TH-C had strongly increased and at TH-A, D, and E the flow had rotated toward Earth. These signatures were the first space indicators of the substorm onset. At #4 the flow at TH-A, D, E had rotated further so that an azimuthal eastward flow component existed. Starting with #5, the flow shows signs of a circular flow pattern at TH-A, D, and E, indicating that a flow vortex had formed. TH-C also shows signs of a passing flow vortex (#5 through #8) in the form of a rotation of the single flow vector. Figure 7 illustrates qualitatively the flow patterns recorded by spacecraft traversing a flow vortex from three different directions (dashed lines). A simple solid-body rotation with a velocity profile indicated in the center is assumed. As can be seen in Figure 7, the flow pattern can be quite variable. The three flow patterns can

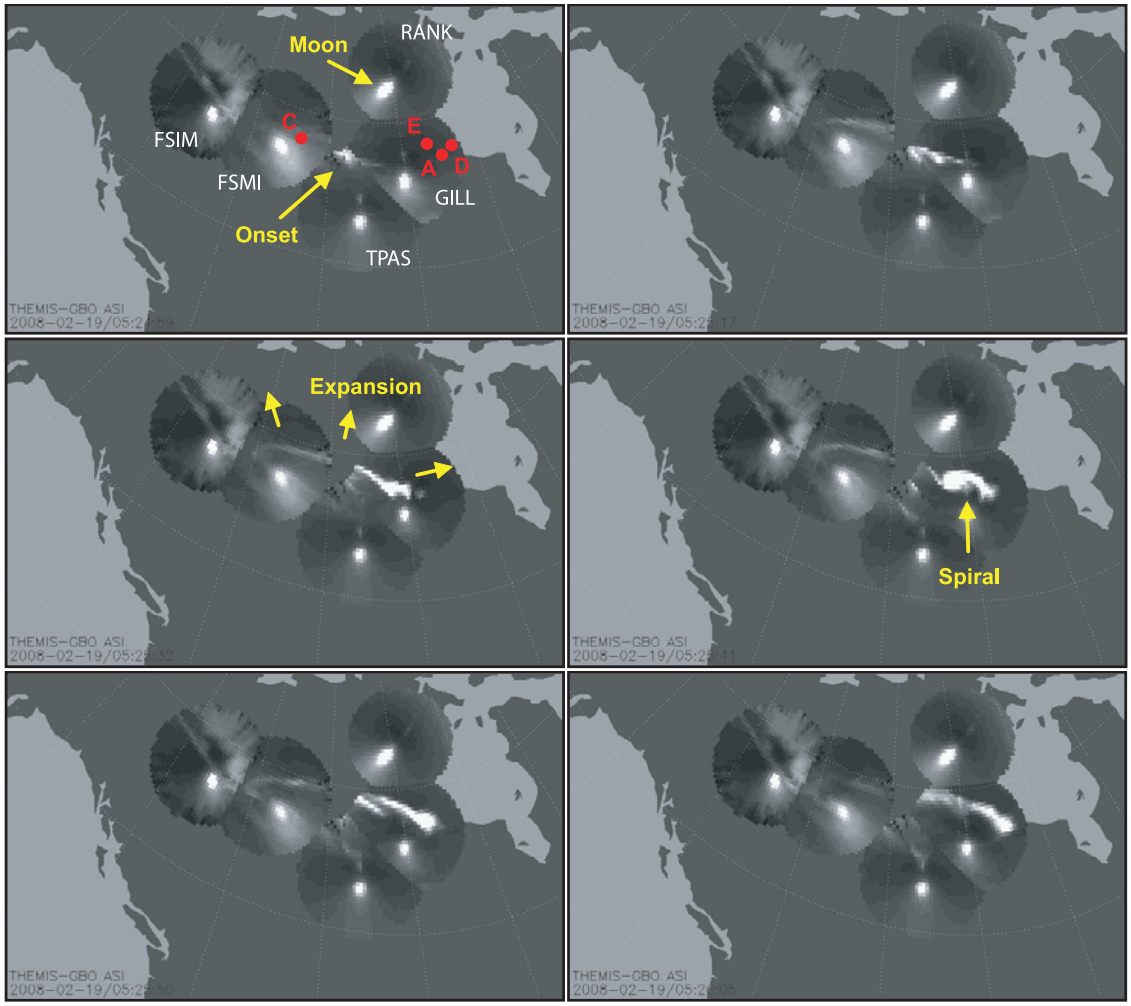

Figure 2. A sequence of ASI images for the substorm on 19 February 2008 with explanation labels in different colors. The red circles are the footprints of the THEMIS spacecraft. Each ASI field of view is approximately 800 km when mapped to a 110-km altitude.

indeed be seen for the four spacecraft (right in Figure 6). Particularly, it is interesting to note that depending on which side the vortex is traversed, the rotation of the flow vector can have the opposite sense (compare paths 1 and 2 with TH-A and TH-D of Figure 6). It is noted that time delays and amplitude variations, as seen in Figure 6, are not exactly reproduced in Figure 7, which suggests that the flow vortex is not simply a solid vortex. Furthermore, although not confirmed, it is suggestive that the flow vortex at TH-C has the opposite sense than the vortex at TH-A, D, and E. In section 3, we provide an estimate of the FAC intensity, using equation (2), generated by the forming space vortex at TH-A, D, and E.

[11] Since the three clustered THEMIS spacecraft (TH-A, D, and E), which were engulfed by a downward current plasma vortex, and the downward current EIC vortex were conjugate, a direct comparison of flow vectors at these two locations is attempted in Figure 8. The spacecraft positions relative to each other and the associated plasma flow vectors are rotated (by hand) so that they can be directly compared with the ionospheric plasma flows which point in the opposite directions of the EIC currents (see section 1 for an explanation). Each panel also shows a square which encloses the locations of the THEMIS footprints. For this comparison, we applied the in situ flow vectors that occurred several tens of seconds earlier than the time shown above each panel as to account for possible travel time delays from the space vortex to the ionosphere. The reader is also cautioned that this comparison is only a rough and qualitative attempt since no reliable magnetospheric model exists that would accurately represent the very active expansion time of substorms. Furthermore, the ionospheric plasma flow direction as inferred from EIC is not valid at every point because of gradients in the ionospheric conductance which have not been considered here. Nevertheless, one can identify a remarkable similarity. The ionospheric flow inside the square of Figure 8 (top) is southwestward, which is the same for the projected flow recorded by THEMIS. In Figure 8 (middle), a clear rotation southeastward had occurred in both the ionospheric flow (inside the square) and the space flow. At that time, an EIC vortex had formed. Inside the square of Figure 8 (bottom), it is apparent that the flow speed had significantly increased (note the different current scales in each panel). Similarly, THEMIS recorded faster plasma flow. In addition, the space flow showed signs of a vortex which

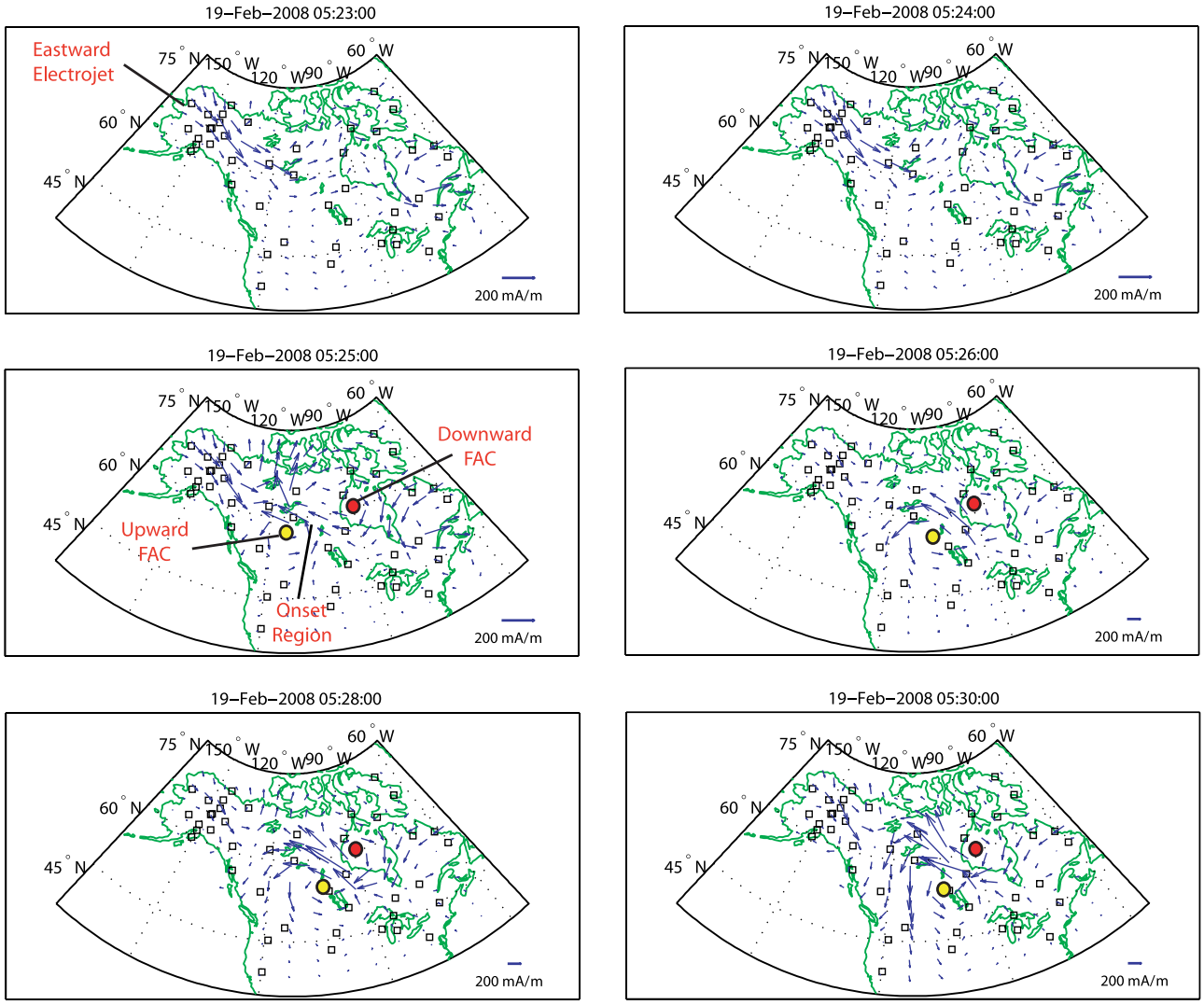

Figure 3. Equivalent ionospheric currents (EICs) for different times during the substorm on 19 February 2008. Red and yellow circles indicate inferred downward and upward currents, respectively.

can be argued is associated with the EICs vortex seen inside the square.

[12] Figure 9 shows an expanded view of the plasma velocities recorded by the THEMIS spacecraft together with keograms from FSMI and GILL. Both ground stations were close to the footprints of TH-C and the clustered TH-A, E, and D, respectively (see Figure 2 for spacecraft footprints and locations of stations). As mentioned earlier, a strong flow (X component) occurred first at TH-C, and then at the cluster TH-E, A, and D. On the ground, FSMI recorded the auroral expansion first followed by GILL (see keograms in Figure 9). The onset time delay between TH-C and FSMI was approximately 1 min (see yellow and black dashed lines), which is comparable to the Alfvén transit time from 9 to 11 R_E in the magnetotail to the ionosphere. Approximately the same delay was observed between TH-A and GILL (yellow and black dashed lines). The ion flow velocities were calculated from the ESA instrument [*McFadden et al.*, 2008] which covers energies from a few eV to 25 keV. During injection events, the energy of the bulk plasma can exceed this energy range. This was the case for the plasma recorded by TH-E, where almost the entire ion population was raised in energy above the ESA threshold (not shown). Hence, we also consulted data from the SST instrument (35 keV–~500 keV (Larson et al., manuscript in preparation, 2009)) to compute the flow velocity by combining data from both instruments. This estimate is shown as a dashed line in Figure 9f, which shows that the sharp drop in the ESA flow velocity at approximately 0525:15 UT was simply due to this ion energization. (Note that the flow vectors in Figure 6 utilize the combined velocity from ESA and SST as described here.)

3. Summary and Discussion

[13] The substorm on 19 February 2008 developed a substorm surge that propagated poleward, westward, and eastward which is typical for substorms [*Akasofu*, 1976], but it is the westward traveling surge which typically causes the most intense aurora. However, on this day the eastward expansion of the brightening region was dominant with a

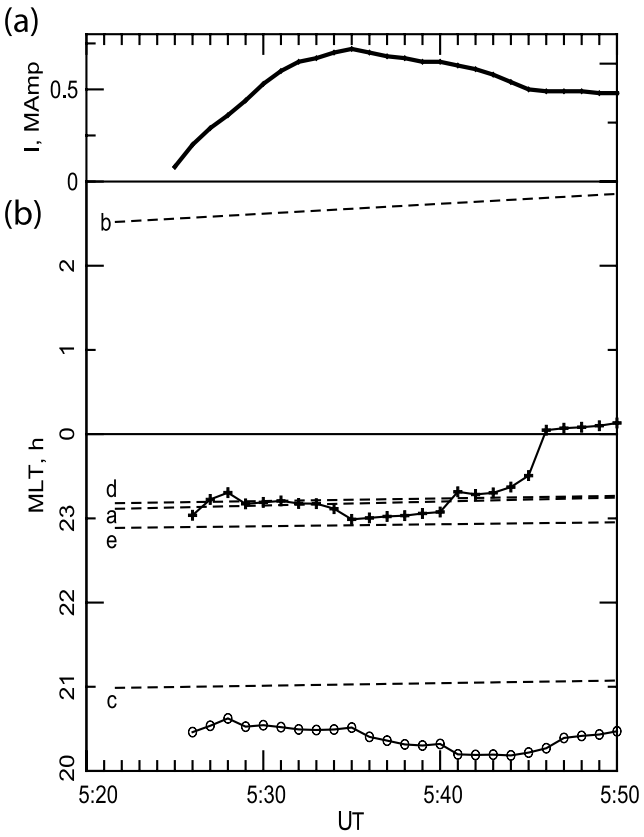

Figure 4. Reconstructed substorm current wedge (SCW) using THEMIS and INTERMAGNET ground magnetometer data. The longitudinal locations of upward and downward FACs as well as their magnitude as a function of time were modeled to fit the midlatitude magnetic variations. (a) Intensity of SCW. (b) Longitude in MLT of downward FAC (crosses), upward FAC (circles), and footprints of TH-A, B, C, D, and E (dashed lines).

speed of ~9 km/s, as inferred from ASI images and resembled an eastward traveling surge. This speed is in the range of earlier reports showing up to 10 km/s for both westward and eastward propagation [e.g., *Steen and Collis*, 1988]. Associated with the eastward expansion on 19 February 2008 was a pair of vortices in EICs with opposite rotational sense, that is, each vortex was associated with an FAC of opposite direction [e.g., *Opgenoorth et al.*, 1980]. The auroral onset occurred at the northern edge of the upward current EIC vortex. The center of the upward current vortex moved eastward after onset while the downward current vortex remained nearly stationary. Simultaneously, four THEMIS spacecraft monitored in situ the conjugate space vortices. One space vortex engulfed the three clustered spacecraft, which were separated in a triangular-like constellation (~1–2 R_E), allowing an unambiguous identification of a counterclockwise flow. The associated clockwise vortex was tentatively inferred from the single spacecraft located further west. The rotational senses of the space vortices were consistent with the conjugate ground EIC vortices. The onsets of the space vortices were recorded approximately 1 min before the optical aurora. This delay is consistent with the Alfvén transit time from the spacecraft locations to the ionosphere.

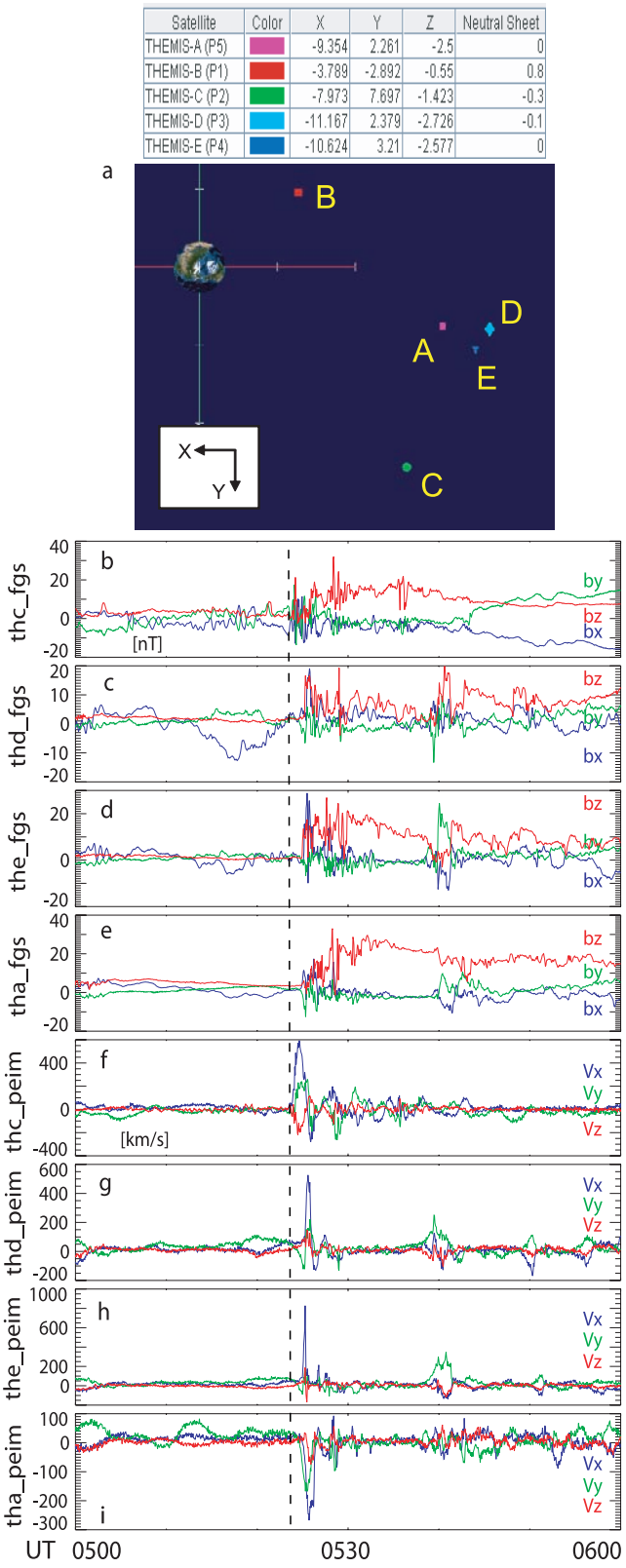

Figure 5. (a) Positions of the THEMIS spacecraft during the substorm on 19 February 2008. Software is provided by http://sscweb.gsfc.nasa.gov/tipsod. (b–e) Magnetic field components and (f–i) plasma flow velocities of TH-A, C, D, and E in GSM coordinates.

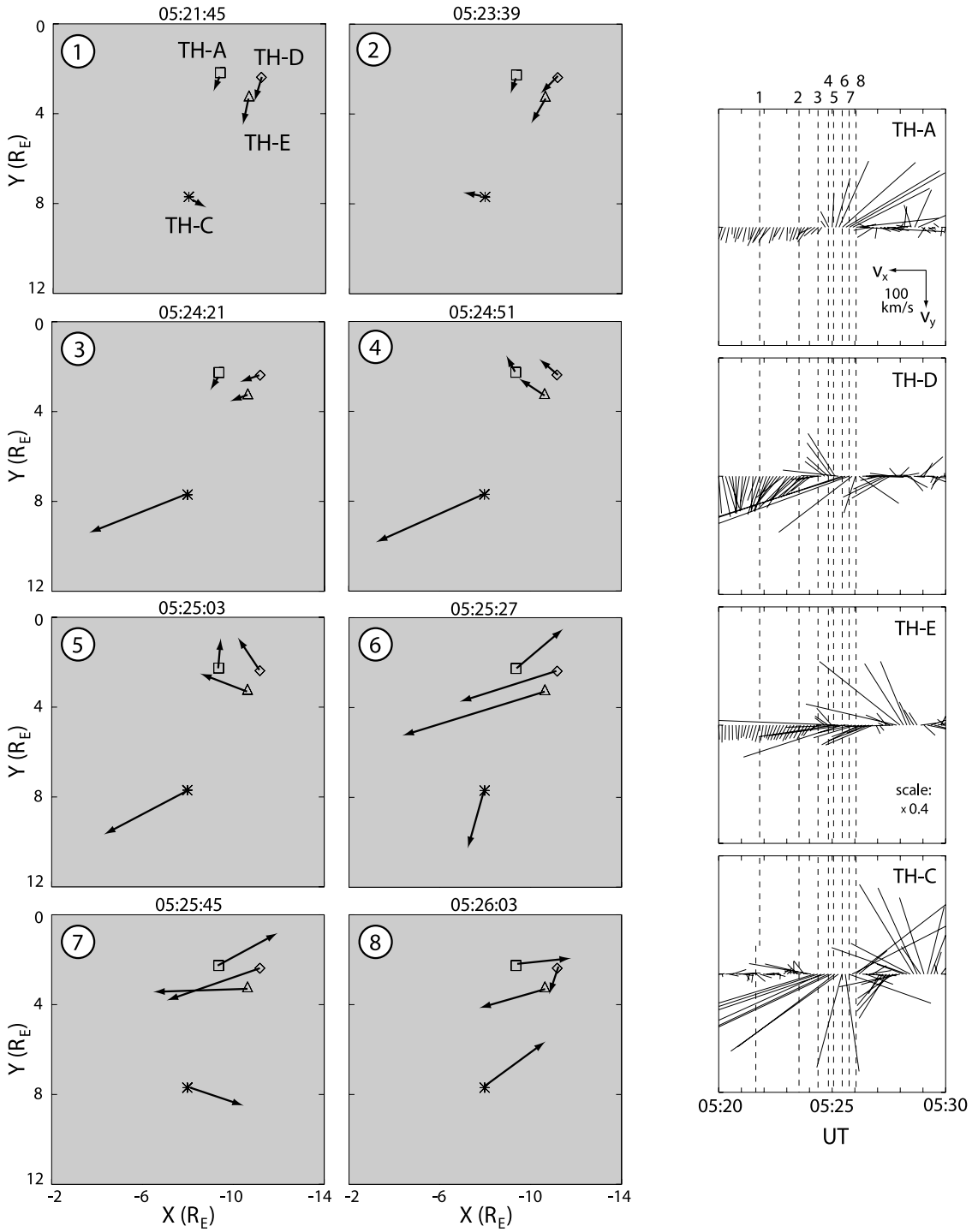

Figure 6. (right) Vector plots of flow velocities (projected onto the X-Y GSM plane) for four THEMIS spacecraft. The vector lengths for TH-E are scaled down to 0.4 in comparison to those of the other spacecraft. Numbered vertical dashed lines indicate times which are shown in Figure 6 (left). (left) THEMIS spacecraft positions overlaid with flow vectors. The times of each snapshot are indicated in Figure 6 (right), as denoted by the numbers 1–8 above the first vector plot (TH-A).

[14] Using equation (2) and data from the clustered constellation TH-A, D, and E, we estimate the contribution to the field-aligned current by the counterclockwise-rotating space vortex. Equation (2) shows that temporal changes of vorticity, $d\Omega/dt$, and the magnetic field, dB/dt, contribute to the current. To isolate the effect of the vorticity, we use a simplified expression which assumes a uniform, incompressible plasma [*Sato and Iijima*, 1979]:

$$j_{\parallel} = \int \rho/B \; d\Omega/dt \; dl_{\parallel} \tag{4}$$

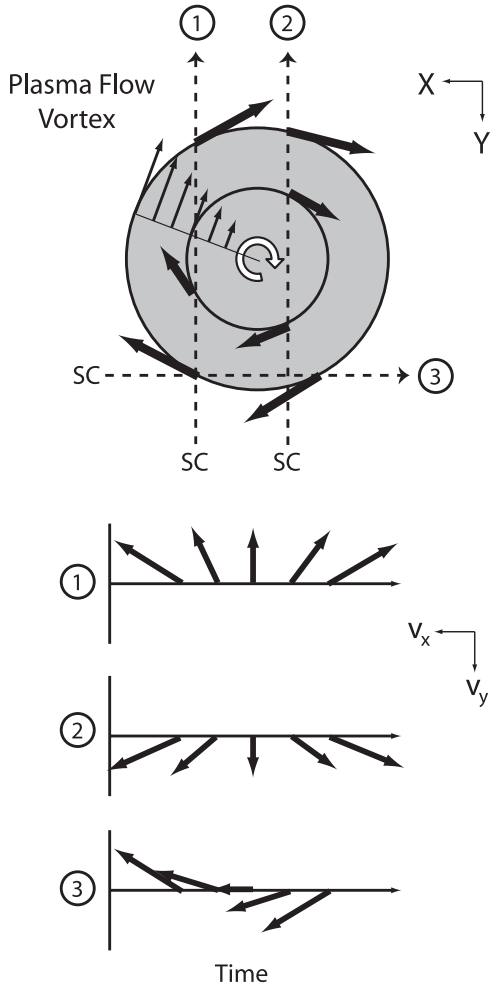

Figure 7. Cartoon of a "solid-body" plasma flow vortex in the equatorial plane as seen from above in the Northern Hemisphere. The bottom three graphs show the velocity vectors versus time recorded by a spacecraft (SC) following trajectories 1, 2, and 3. The length and direction of each vector are only qualitatively accurate.

The symbols are the same as for equation (2). An approximation of (4), assuming all quantities are constant inside the vortex and do not vary with time except vorticity, is

$$j_{\parallel} \approx 2 \cdot \left(n\, m_H / B_{eq,avg}\right)\left(v_{final}/\tau\right)(L/r) \qquad (5)$$

In addition, we used the assumption of a solid-body rotation for the vortex, that is, $\Omega = 2 \cdot v/r$ (Figure 7). Using $B_{eq,avg}$ = 10 nT (approximate value of the equatorial magnetic field averaged over the three spacecraft near the beginning of the vortex formation), v_{final} = 500 km/s (approximate final rotational vortex speed averaged over three spacecraft), r = 1 R_E (radius of vortex), L = 1 R_E (vertical scale height), τ = 30 s (formation time of vortex), and n = 1/cc, we obtain a current density in the equatorial region of approximately 5.6 nA/m^2 or a total current of 2.2 $\times$ 10^5 A using a cross-sectional area of 1 R_E^2. Note that it is not necessary to integrate along the entire field line from the equator to the ionosphere, as indicated in equation (2), because most of the plasma flow is typically concentrated near the equatorial region surrounded by the region of magnetic field distortion caused by the flow vortex [*Birn and Hesse*, 1996].

[15] From Figure 5, it can be seen that both the vortex formation (enhanced flows) and an increase in **B** (dipolarization) occurred simultaneously. Including the effect of a changing magnetic field, dB/dt, see (2), and using zero vorticity at the start of the integration, an approximation of the equatorial current density yields

$$j_{\parallel} \approx 2 \cdot \left(n\, m_H / B_{eq,final}\right)\left(v_{final}/\tau\right)(L/r) \qquad (6)$$

Here $B_{eq,final}$ expresses the amount of change of **B**. Comparing (5) and (6) suggests that (6) could also be interpreted as describing a vortex with a constant magnetic field of $B_{eq,final}$. Using $B_{eq,final}$ = 20 nT (from Figure 5), we obtain a current density of about 2.8 nA/m^2 or a total current of 1.1 $\times$ 10^5 A, again using a cross-sectional area of 1 R_E^2.

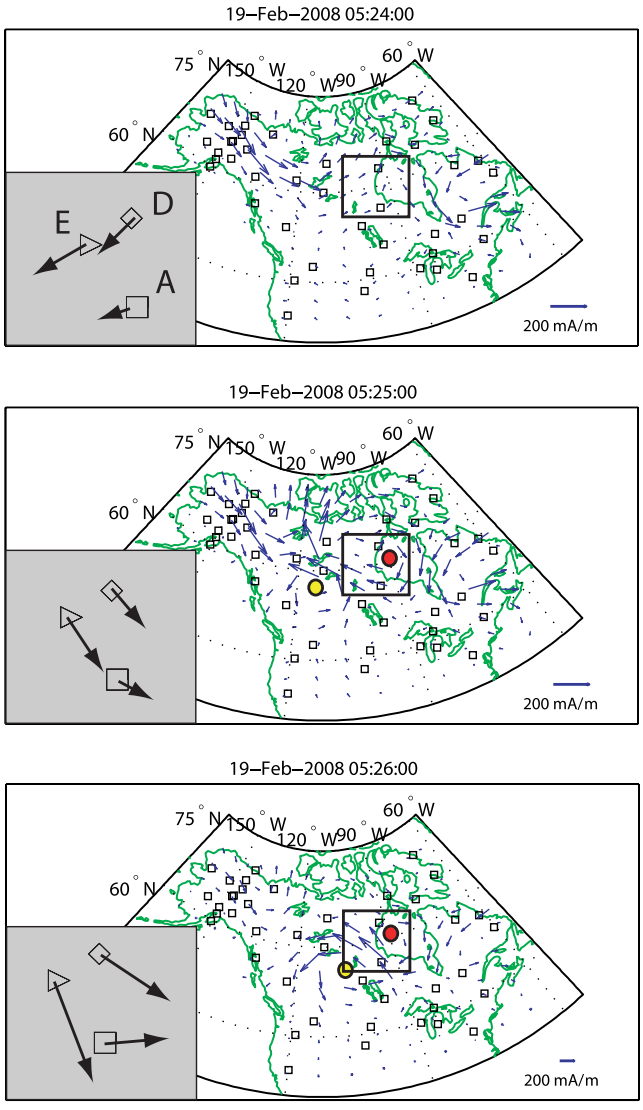

Figure 8. Comparison of conjugate flows in the ionosphere as inferred from EICs (note: the opposite of the EIC directions yields an estimate of the ionospheric plasma flow direction) and in space as measured by THEMIS. The selected panels are a subset of those in Figure 3.

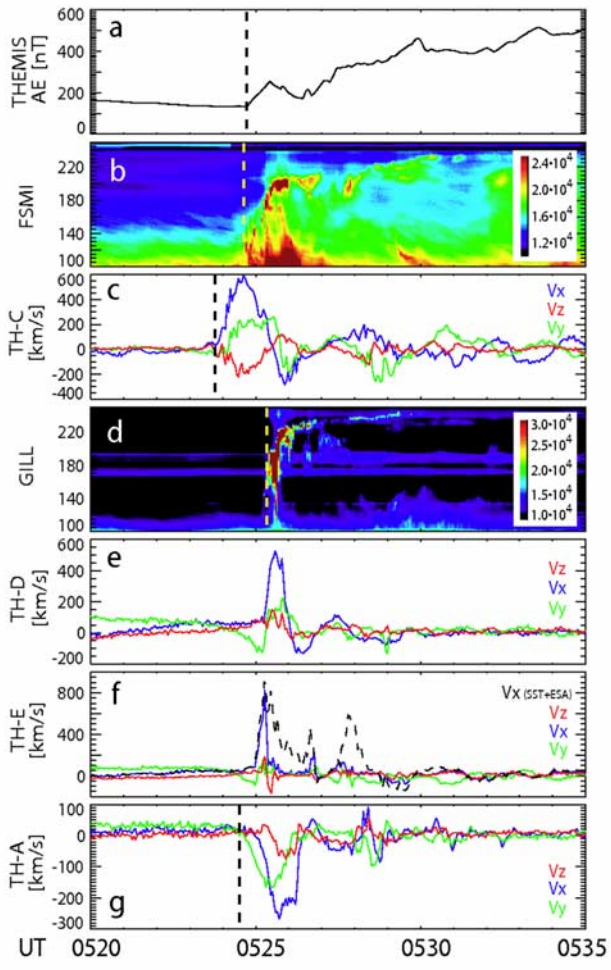

Figure 9. Comparison of optical signatures and flow velocities. (a) THEMIS AE index (calculated from THEMIS ground stations only). (b and d) Keograms taken at Fort Smith (FSMI) and Gillam (GILL). The intense luminosity around 100° is due to the Moon. (c and e–g) Flow velocities for four THEMIS spacecraft determined from the ESA instrument. The dashed line in Figure 9f indicates the flow velocity determined from both the ESA and SST instrument data (see text for additional information).

This shows that the increase in **B** has a current-reduction effect on the vortex-generated field-aligned current. In comparison, the modeled SCW (Figure 4) showed a gradual increase in current with a peak value of $\sim 7 \times 10^5$ A about 10 min after onset, and a downward current that longitudinally coincided with the space vortex. Closer to the time of the space vortex observations, the modeled current was between 1 and 2×10^5 A. Therefore, this comparison suggests that the space vortex contributed a significant part or all of the FAC of the SCW at onset of the substorm expansion phase, which could later be replaced by other current-generating mechanisms such as the pressure gradient [e.g., *Birn et al.*, 1999].

[16] Earlier studies [*Shiokawa et al.*, 1997; *Kepko et al.*, 2001], using the expression for the inertial current in equation (1), have given slightly smaller values of 0.3–0.7×10^5 A for the initial substorm current. These studies did not compare their current estimates with the peak current of the investigated substorms, however, so that no comparison with the substorm reported here regarding its peak intensity can be made. In spite of the small differences to these studies, we find our result comparable, since both their and our estimates rely on approximate values which could not be measured and thus must be used with caution. Similarly, the assumption of a solid-body vortex is not valid, and a more realistic velocity distribution is unobtainable even in the near future since it would require many more spacecraft, simultaneously probing the space vortex. Here, the novel result is the calculation of the substorm current by direct application of (2) which relates the field-aligned current generation to the forming space vortex. Other effects also generate field-aligned currents (compare section 1). For example, *Lui* [1996] estimated the field-aligned current density due to the gradient in the magnetic field inside the current disruption region at substorm onset [see also *Hasegawa and Sato*, 1979] and reported 4 μA/m^2 at the ionospheric level, which is comparable to the mapped current density caused by the space vortex reported here, namely 14 μA/m^2 (shown in the next paragraph).

[17] The space dimensions and the current density of the flow vortex at the magnetic equator can be mapped to the upper ionosphere using $R_i/R_e = M^{-0.5}$ and $j_i/j_e = M$, where the subscripts "i" and "e" denote ionospheric and equatorial quantities, and M is the mirror ratio [*Robert et al.*, 1984]. Using M = 5000, we obtain for the ionospheric counterpart 14 μA/m^2 (2.8 nA/m^2 at the equator) and 180 km in diameter. This current density is in the range of observed low-altitude values which have been associated with downward currents and also with auroral arcs [e.g., *Aikio et al.*, 2002, and references therein]. *Stasiewicz and Potemra* [1998] showed that current densities can vary over a large range and correspond to different spatial scales. Using their results, a current density of 14 μA/m^2 would correspond to a spatial scale closer to 100 km. However, here we cannot verify whether the current generated in the magnetosphere at the equatorial region was possibly striated into smaller current structures at lower altitudes due to magnetosphere-ionosphere coupling processes. Regarding the mapping of a flow vortex from the magnetosphere to the ionosphere, *Borovsky and Bonnell* [2001] showed theoretically that the ionospheric footprint of a positive (downward current) vortex is larger than the mapped footprint of the corresponding magnetospheric vortex because of a spreading of the associated electric potential from high to low altitude. Hence, the larger EIC vortex (~600–800 km reported here) versus the smaller mapped footprint (~180 km) could be explained by this spreading and/or because the THEMIS spacecraft did not enclose the entire space vortex. Assuming conservation of angular speed, the flow speed of 300–900 km/s corresponds to 4–12 km/s in the ionosphere. However, this assumption is most likely not valid because of ionospheric drag, and thus the mapped speeds should only be considered as an upper limit.

[18] The combined ground and space observations suggest a scenario in which both EIC vortices were directly driven by two space vortices as illustrated in Figure 10, which follows from the good ground-space correlations of the following features: (1) conjugacy of ionospheric and space vortices, (2) same rotational sense of conjugate

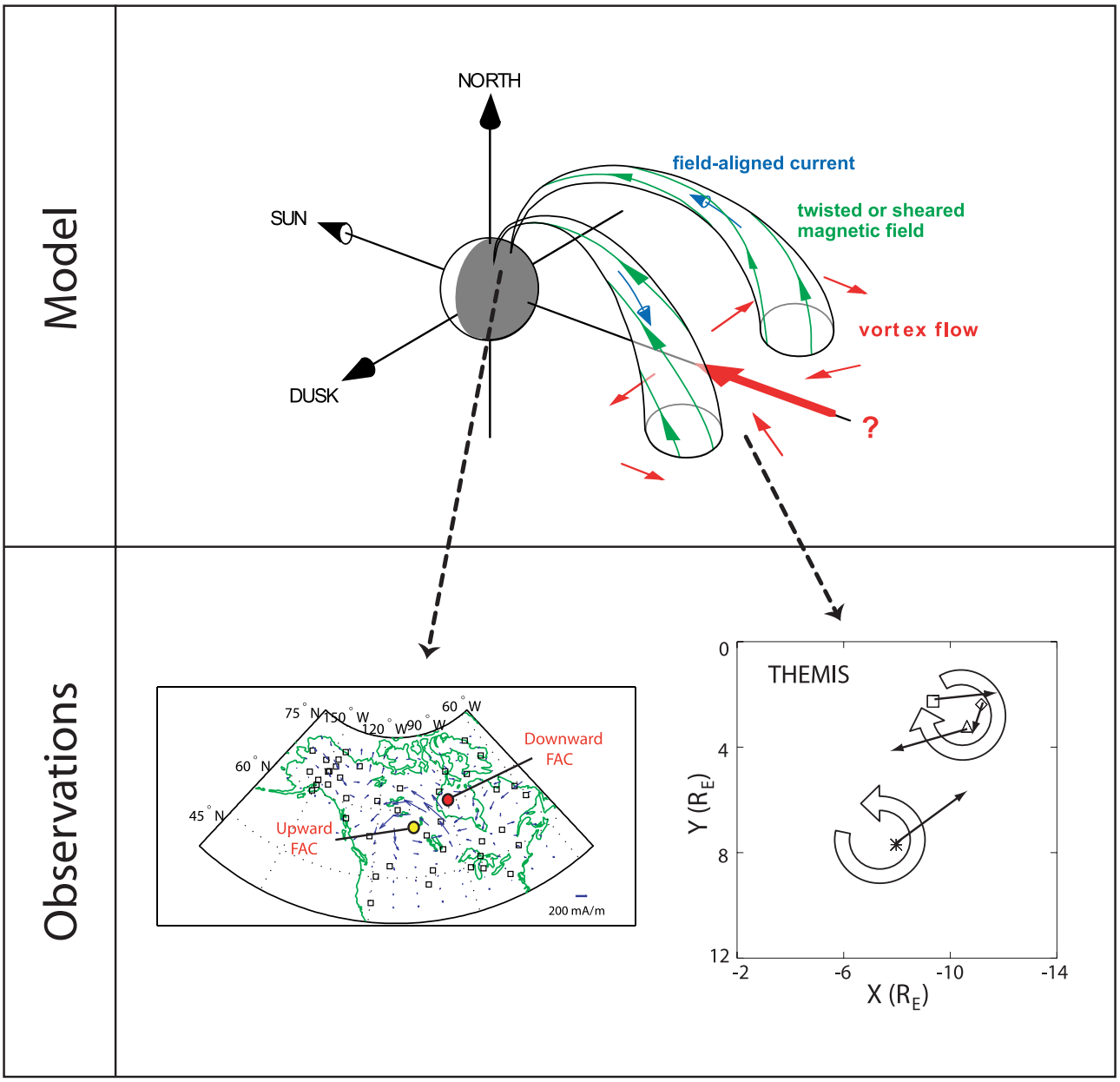

Figure 10. Model and observations demonstrating the connection of two flow vortices in space to two EIC vortices in the ionosphere. The cartoon at the top is modified from *Birn et al.* [2004].

vortices, and (3) consistency of Alfvén wave travel time and onset delay between ionosphere and space. Significantly, we provided observational evidence that flow vortices in space contribute to the SCW, likely by launching Alfvén waves which carry the FAC toward the ionosphere. What created the space vortices is a different question and has not been investigated in this study. Here we only mention briefly two competing models. Earlier studies have suggested that bursty bulk flows and ballooning instability could provide the disturbance which lead to vortex formation [e.g., *Angelopoulos et al.*, 1996; *Voronkov et al.*, 1997; *Shiokawa et al.*, 1997; *Birn et al.*, 2004]. The vortex cartoon shown in Figure 10 has been proposed for bubbles in the magnetotail [*Birn et al.*, 2004]. However, an application of this scenario to vortex formation in the near-Earth plasma sheet (~10–12 R_E) could be envisioned as well. An abrupt interchange of plasma (ballooning instability) causing both vortices is likely, too.

[19] Finally, we reported a large auroral spiral (~300 km) during the substorm on 19 February 2008. The auroral spiral was among the brightest auroral features and formed between the two EIC vortices, approximately at the time when they reached their closest separation. The region between both vortices was a region of strong flow as inferred from the EICs. An association of strong shear flow and auroral spiral has long been suggested [e.g., *Steen and Collis*, 1988] and later by others [e.g., *Voronkov et al.*, 1997]. The EIC vortices on 19 February 2008 lasted longer than the auroral spiral, suggesting that the strong flow is not the only criterion for auroral spiral formation. Additional analysis of the auroral spiral will be presented in a separate study.

[20] **Acknowledgments.** This work was supported by the NASA THEMIS project (NAS5-02099). The work of the IGEP team at the Technical University of Braunschweig was financially supported by the German Ministerium für Wirtschaft und Technologie and the German Zentrum für Luft- und Raumfahrt under grant 50QP0402. One of the authors (A.K.) thanks Yan Song for valuable discussions.

[21] Wolfgang Baumjohann thanks Kazuo Shiokawa and Joachim Vogt for their assistance in evaluating this paper.

References

Aikio, A. T., T. Lakkala, A. Kozlovsky, and P. J. S. Williams (2002), Electric fields and currents of stable drifting auroral arcs in the evening sector, *J. Geophys. Res.*, *107*(A12), 1424, doi:10.1029/2001JA009172.

Akasofu, S.-I. (1976), *Physics of Magnetospheric Substorms*, D. Reidel, Dordrecht, Netherlands.

Amm, O. (1997), Ionospheric elementary current systems in spherical coordinates and their application, *J. Geomagn. Geoelectr.*, *49*, 947–955.

Amm, O., and A. Viljanen (1999), Ionospheric disturbance magnetic field continuation from the ground to the ionosphere using spherical elementary current systems, *Earth Planets Space*, *51*, 431–440.

Angelopoulos, V. (2008), The THEMIS mission, *Space Sci. Rev.*, *141*, 5–34, doi:10.1007/s11214-008-9336-1.

Angelopoulos, V., et al. (1996), Multipoint analysis of a bursty bulk flow event on April 11, 1985, *J. Geophys. Res.*, 101, 4967, doi:10.1029/95JA02722.

Ashour-Abdalla, M., M. El-Alaoui, F. V. Coroniti, R. J. Walker, and V. Peroomian (2002), A new convection state at substorm onset: Results from an MHD study, *Geophys. Res. Lett.*, *29*(20), 1965, doi:10.1029/2002GL015787.

Auster, H. U., et al. (2008), The THEMIS fluxgate magnetometer, *Space Sci. Rev.*, *141*, 235–264, doi:10.1007/s11214-008-9365-9.

Bester, M., M. Lewis, B. Roberts, J. McDonald, D. Pease, J. Thorsness, S. Frey, D. Cosgrove, and D. Rummel (2008), THEMIS operations, *Space Sci. Rev.*, *141*, 91–115, doi:10.1007/s11214-008-9456-7.

Bhattacharjee, A., Z. W. Ma, and X. Wang (1998), Dynamics of thin current sheets and their disruption by ballooning instabilities: A mechanism for magnetospheric substorms, *Phys. Plasmas*, *5*, 2001–2009, doi:10.1063/1.872871.

Birn, J. M., and M. Hesse (1996), Details of current disruption and diversion in simulations of magnetotail dynamics, *J. Geophys. Res.*, *101*, 15,345–15,358, doi:10.1029/96JA00887.

Birn, J., M. Hesse, G. Haerendel, W. Baumjohann, and K. Shiokawa (1999), Flow braking and the substorm current wedge, *J. Geophys. Res.*, *104*, 19,895–19,903, doi:10.1029/1999JA900173.

Birn, J. M., et al. (2004), On the propagation of bubbles in the magnetotail, *Ann. Geophys.*, *22*, 1773–1786.

Borovsky, J. E., and J. W. Bonnell (2001), The DC electrical coupling of flow vortices and flow channels in the magnetosphere to the resistive ionosphere, *J. Geophys. Res.*, *106*, 28,967–28,994, doi:10.1029/1999JA000245.

Haerendel, G. (1992), Disruption, ballooning or auroral avalanche—On the cause of substorms, in *Proceedings of the International Conference on Substorms (ICS-1)*, *Eur. Space Agency Spec. Publ., ESA SP-335*, pp. 417–420.

Hasegawa, A., and T. Sato (1979), Generation of field aligned current during substorm, in *Dynamics of the Magnetosphere*, edited by S.-I. Akasofu, pp. 529–542, D. Reidel, Norwell, Mass.

Horning, B. L., R. L. McPherron, and D. D. Jackson (1974), Application of linear inverse theory to a line current model of substorm current systems, *J. Geophys. Res.*, *79*(34), 5202–5210, doi:10.1029/JA079i034p05202.

Kepko, L., et al. (2001), Flow bursts, braking, and Pi2 pulsations, *J. Geophys. Res.*, *106*, 1903–1915, doi:10.1029/2000JA000158.

Kosch, M. J., M. W. J. Scourfield, and E. Nielsen (1998), A self-consistent explanation for a plasma flow vortex associated with the brightening of an auroral arc, *J. Geophys. Res.*, *103*, 29,383–29,391, doi:10.1029/98JA02480.

Kosch, M. J., et al. (2000), A plasma vortex revisited: The importance of including ionospheric conductivity measurements, *J. Geophys. Res.*, *105*, 24,889–24,898, doi:10.1029/2000JA900102.

Küppers, F., J. Untiedt, W. Baumjohann, K. Lange, and A. G. Jones (1979), A two-dimensional magnetometer array for ground-based observations of auroral zone electric currents during the international magnetospheric study (IMS), *J. Geophys.*, *46*, 429–450.

Lui, A. T. Y. (1996), Current disruption in the Earth's magnetosphere: Observations and models, *J. Geophys. Res.*, *101*, 13,067–13,088, doi:10.1029/96JA00079.

Lui, A. T. Y., et al. (1991), A cross-field current instability for substorm expansions, *J. Geophys. Res.*, *96*, 11,389–11,401, doi:10.1029/91JA00892.

Lyatsky, W., L. L. Cogger, B. Jackel, A. M. Hamza, W. J. Hughes, D. Murr, and O. Rasmussen (2001), Substorm development as observed by Interball UV imager and 2-D magnetic array, *J. Atmos. Sol. Terr. Phys.*, *63*, 1609–1621, doi:10.1016/S1364-6826(01)00045-1.

McFadden, J. P., C. W. Carlson, D. Larson, M. Ludlam, R. Abiad, B. Elliott, P. Turin, M. Marckwordt, and V. Angelopoulos (2008), The THEMIS ESA plasma instrument and in-flight calibration, *Space Sci. Rev.*, *141*, 277–302, doi:10.1107/s11214-008-9440-2.

McPherron, R. L. (1979), Magnetospheric substorms, *Rev. Geophys. Space Phys.*, *17*, 657–681, doi:10.1029/RG017i004p00657.

Mende, S. B., S. E. Harris, H. U. Frey, V. Angelopoulos, C. T. Russell, E. Donovan, B. Jackel, M. Greffen, and L. M. Peticolas (2008), The THEMIS array of ground-based observatories for the study of auroral substorms, *Space Sci. Rev.*, *141*, 357–387, doi:10.1007/s11214-008-9380.

Opgenoorth, H. J., R. J. Pellinen, H. Maurer, F. Küppers, W. J. Heikkila, and P. Tanskanen (1980), Ground-based observations of an onset of localized field-aligned currents during auroral breakup around magnetic midnight, *J. Geophys.*, *48*, 101–115.

Pudovkin, M. I., et al. (1997), Vorticity in the magnetospheric plasma and its signatures in the aurora dynamics, *Space Sci. Rev.*, *80*, 411–444, doi:10.1023/A:1004916808514.

Robert, P., et al. (1984), GEOS 2 identification of rapidly moving current structures in the equatorial outer magnetosphere during substorms, *J. Geophys. Res.*, *89*, 819–840, doi:10.1029/JA089iA02p00819.

Russell, C. T., P. J. Chi, D. J. Dearborn, Y. S. Ge, B. Kuo-Tiong, J. D. Means, D. R. Pierce, K. M. Rowe, and R. C. Snare (2008), THEMIS ground-based magnetometers, *Space Sci. Rev.*, *141*, 389–412, doi:10.1007/s11214-008-9337-0.

Sato, T., and T. Iijima (1979), Primary sources of large-scale Birkeland currents, *Space Sci. Rev.*, *24*, 347–366, doi:10.1007/BF00212423.

Sergeev, V. A., et al. (1996), Comparison of UV optical signatures with the substorm current wedge as predicted by an inversion algorithm, *J. Geophys. Res.*, *101*(A2), 2615–2627, doi:10.1029/95JA00537.

Shiokawa, K., W. Baumjohann, and G. Haerendel (1997), Braking of high-speed flows in the near-Earth tail, *Geophys. Res. Lett.*, *24*, 1179–1182, doi:10.1029/97GL01062.

Sibeck, D. G., and V. Angelopoulos (2008), THEMIS science objectives and mission phases, *Space Sci. Rev.*, *141*, 35–59, doi:10.1007/s11214-008-9393-5.

Stasiewicz, K., and T. Potemra (1998), Multiscale current structures observed by Freja, *J. Geophys. Res.*, *103*, 4315–4325, doi:10.1029/97JA02396.

Steen, A., and P. N. Collis (1988), High-time resolution imaging of auroral arc deformation at substorm onset, *Planet. Space Sci.*, *36*, 715–732, doi:10.1016/0032-0633(88)90120-1.

Tsyganenko, N. A. (1995), Modeling the Earth's magnetospheric magnetic field confined within a realistic magnetopause, *J. Geophys. Res.*, *100*, 5599–5612, doi:10.1029/94JA03193.

Untiedt, J., R. Pellinen, F. Küppers, H. J. Opgenoorth, W. D. Pelster, W. Baumjohann, H. Ranta, J. Kangas, P. Czechowsky, and W. J. Heikkila (1978), Observations of the initial development of an auroral and magnetic substorm at magnetic midnight, *J. Geophys.*, *45*, 41–56.

Voronkov, I., et al. (1997), Coupling of shear flow and pressure gradient instabilities, *J. Geophys. Res.*, *102*, 9639–9650, doi:10.1029/97JA00386.

Weygand, J. M., R. L. McPherron, H. Frey, O. Amm, K. Kauristie, A. T. Viljanen, and A. Koistinen (2008), Relation of substorm onset to Harang discontinuity, *J. Geophys. Res.*, *113*, A04213, doi:10.1029/2007JA012537.

O. Amm, Finnish Meteorological Institute, P.O. Box 503, FIN-00101 Helsinki, Finland.

V. Angelopoulos, A. Runov, and J. Weygand, IGPP, University of California, Los Angeles, CA 90095, USA.

S. V. Apatenkov, Institute of Physics, St. Petersburg State University, Ulyanovskya 1, Petrodvoretz, St. Petersburg 198504, Russia.

H. U. Auster and K.-H. Glassmeier, IGEP, Technical University of Braunschweig, Mendelssohnstrasse 3, D-38106 Braunschweig, Germany.

A. Keiling, D. Larson, S. Mende, and J. McFadden, Space Sciences Laboratory, University of California, 7 Gauss Way, Berkeley, CA 94720, USA. (keiling@ssl.berkeley.edu)